Direct probe of linearly dispersing 2D interband plasmons in a free-standing graphene monolayer

2012 EPL 97 57005

(http://iopscience.iop.org/0295-5075/97/5/57005)

A Letters Journal Exploring the Frontiers of Physics

March 2012

EPL, **97** (2012) 57005
doi: 10.1209/0295-5075/97/57005

www.epljournal.org

Direct probe of linearly dispersing 2D interband plasmons in a free-standing graphene monolayer

M. K. Kinyanjui[1(a)], C. Kramberger[2], T. Pichler[2], J. C. Meyer[1(b)], P. Wachsmuth[1], G. Benner[3] and U. Kaiser[1]

[1] *University of Ulm, Central Facility of Electron Microscopy - Albert-Einstein-Allee 11, D-89081 Ulm, Germany, EU*
[2] *University of Vienna, Faculty of Physics - Strudlhofgasse 4, A-1090 Vienna, Austria, EU*
[3] *Carl Zeiss NTS GmbH - Carl-Zeiss-Str. 56, D-73447 Oberkochen, Germany, EU*

received on 11 January 2012; accepted by J. Fink on 26 January 2012
published online 2 March 2012

PACS 78.67.-n – Optical properties of low-dimensional, mesoscopic, and nanoscale materials and structures
PACS 78.67.Wj – Optical properties of graphene
PACS 73.20.Mf – Collective excitations (including excitons, polarons, plasmons and other charge-density excitations)

Abstract – In low-dimensional systems, a detailed understanding of plasmons and their dispersion relation is crucial for applying their optical response in the field of plasmonics. Electron energy-loss spectroscopy is a direct probe of these excitations. Here we report on electron energy-loss spectroscopy results on the dispersion of the π plasmons in free-standing graphene monolayers at the momentum range of $0 \leqslant |\boldsymbol{q}| \leqslant 0.5\,\text{Å}^{-1}$ and parallel to the Γ-M direction of the graphene Brillouin zone. In contrast to the parabolic dispersion in graphite and in good agreement with theoretical predictions of a 2D electron gas of Dirac electrons, linear π plasmon dispersion is observed. As with previous EELS results obtained from single-wall carbon nanotubes, this can be explained by local-field effects in the anisotropic 2D system yielding a significant contribution of the low-energy band structure on the high-energy π plasmon response.

Introduction. – The unique electronic and structural properties of two-dimensional (2D) graphene have caused a lot of excitement recently. At low energies charge carriers in graphene are a massless 2D gas of Dirac electrons which results in unique electronic and structural properties including extremely high charge mobility, fractional quantum Hall effect among others [1,2]. Furthermore, graphene is considered to be the basic structural unit of several forms of carbon including fullerenes, single-wall carbon nanotubes (SWCNT) and graphite [3–5]. Recently a lot of interest has also been focussed on the nature of 2D plasmons in graphene [3,6–19]. 2D plasmons can be broadly described as collective excitations of charge density localized on a 2D system [20]. Plasmon oscillations are a result of Coulomb interaction between electrons and can be described based on their dispersion relation (dependence of plasmon wavelength on energy) [21]. Insights into the nature of 2D plasmons in graphene are not only important for the fundamental understanding of the electronic structure and collective behaviour in graphene, but also for potential applications in nano-plasmonics [2,22]. This paper is concerned with the dispersion of high-energy interband plasmons also known as π plasmons in free-standing graphene monolayer.

Studies on plasmons in graphene have mainly focused on the low-energy plasmons (or charge carrier plasmons) which occur at 0–3 eV. The reason being the position and dispersion of these charge carrier plasmons is directly related to the electronic transport properties [2]. In addition all these studies are based on epitaxial graphene on semi-conducting or metallic substrates. This includes graphene on semiconducting SiC (0001) substrate [9,10,12,18], and on metallic Ir (111) [11], Pt (111) [13], Ni (111) and Au/Ni (111) [14] substrates. However, much less is known about the nature of π and $\pi + \sigma$ plasmons which are observed at higher energies, above 4 eV and 14 eV, respectively. While several papers including Mak *et al.* [15], Eberlein *et al.* [16], and Yuan *et al.* [17]

(a) E-mail: michael.kinyanjui@uni-ulm.de
(b) Present address: University of Vienna, Faculty of Physics - Strudlhofgasse 4, A-1090 Vienna, Austria, EU.

have investigated the position of the π plasmons in epitaxial graphene and free-standing graphene layers, respectively, they did not determine the dispersion of the π plasmon excitation spectrum. As shown by Kramberger *et al.* [3], for individual SWNT, and by Lu *et al.* for epitaxial graphene on SiC (0001) [18], the dispersion of π plasmon excitations yields a lot of new information on the electronic band structure of graphene. Furthermore, the dispersion behaviour of both low-energy and high-energy plasmons in free-standing single- and multi-layer graphene is yet to be investigated. In this paper, we present the first experimental study on the dispersion properties of π plasmons in free-standing graphene monolayers. For this we have applied momentum-resolved electron energy-loss spectroscopy (EELS) in the transmission electron microscope (TEM) to determine the plasmon dispersion. This technique is particularly suited to study plasmon dispersion since it can probe electronic excitations at a wider range of momentum transfers [23–25]. Optical spectroscopy is on the other hand restricted to excitations at zero momentum transfer. In addition compared to optical spectroscopy, momentum resolved EELS has a better spatial resolution (in this case $< 200\,\text{nm}$) and can therefore be used to study very small regions of the sample. Our results show that 2D π plasmons in free-standing graphene monolayers have a linear energy-momentum dispersion which is in good agreement with theoretical predictions [3].

Experimental methods. – We prepared the graphene membranes used in this work through the mechanical exfoliation method [26]. We then transferred the graphene membranes onto perforated carbon grids with $1.3\,\mu\text{m}$ holes on 200 mesh gold grids (Quantifoil Micro Tools GmbH, Jena, Germany) for EELS investigations [27]. Our EELS investigations were done on a Libra-based transmission electron microscope prototype (ZEISS) operating at 20 kV [28]. We determined the energy and momentum resolution to be 0.60 eV and $0.05\,\text{Å}^{-1}$, respectively. In the TEM, the graphene layers were placed perpendicular to the incident beam. Figure 1(a) shows an overview TEM bright field image of the graphene layers. The graphene layers are shown in red, the blue regions shows the TEM grid and the holes in the grid are shown in yellow. Investigations were done on free-standing graphene monolayers lying on top of a hole. We acquired selected area electron diffraction patterns from the clean regions of the graphene layers. Monolayers of graphene were then confirmed by the intensity distribution of the electron diffraction spots as described in literature [29]. Figure 1(b) shows an electron diffraction pattern for a graphene monolayer, the arrows mark the position of the (−1 1 0 0) and (1 −1 0 0) diffraction spots. To obtain momentum resolved EELS spectra, a slit placed above the EELS spectrometer was used to select electrons which have been scattered to a particular scattering angle. The area covered by the slit then defines

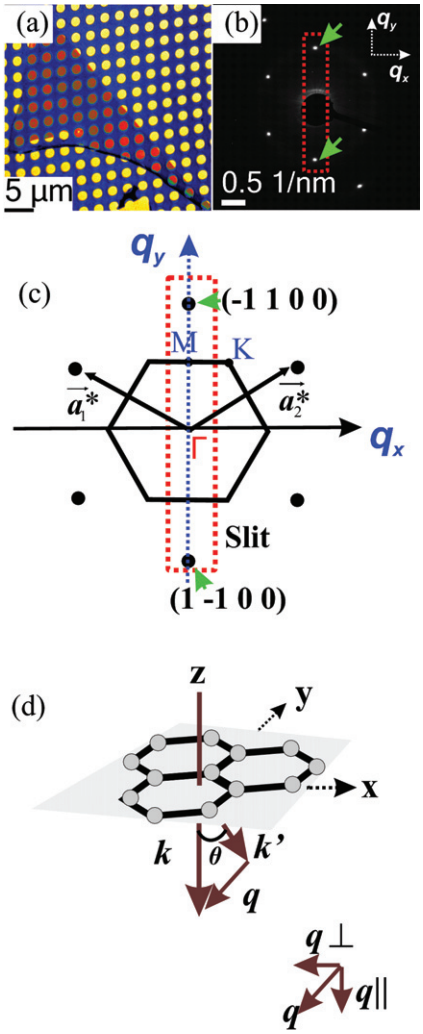

Fig. 1: (a) A false colour TEM bright field image of the graphene layers. The layers are shown in red, blue regions represent the TEM grid and the yellow regions show the holes in the grid. (b) An electron diffraction pattern obtained from a free-standing graphene monolayer. The arrows mark the (−1 1 0 0) and (1 −1 0 0) diffraction spots. The red rectangle shows the position of the selecting slit which was placed along the (−1 1 0 0) and (1 −1 0 0) diffraction spots. (c) A model of the electron diffraction pattern and the Brillouin zone (BZ) for graphene showing that the region selected by the slit (dotted rectangle) is parallel to the Γ-M direction of the BZ. (d) Sample orientation and scattering geometry for the EELS experiments. The scattering vector $\boldsymbol{q}$ is given by $\boldsymbol{k}_0 - \boldsymbol{k}'$ where $\boldsymbol{k}_0$ and $\boldsymbol{k}'$ are the wave vectors of the incident and the inelastically scattered electrons, respectively, and θ is the scattering angle. The vectors $\boldsymbol{q}\,\|$ and $\boldsymbol{q}\,\perp$ are the parallel and perpendicular components of the wave vector $\boldsymbol{q}$, respectively. For the energies losses of interest in this work ($0 \leqslant \Delta E \leqslant 10\,\text{eV}$), the momentum transfer is in the graphene layer plane ($\boldsymbol{q}\,\perp$).

an area in the reciprocal space which is dispersed by the spectrometer to give a momentum resolved EELS spectrum [25]. The red rectangle in fig. 1(b) shows the position of the selecting slit which was placed along the (−1 1 0 0) and (1 −1 0 0) diffraction spots. For

graphene, this corresponds to the Γ-M direction of the graphene Brillouin zone (BZ) as shown in fig. 1(c). In anisotropic materials such as graphene, graphite or boron nitride, the features in the EELS spectra will also depend on the direction of momentum transfer with respect to the graphene layer [30–32]. Sample orientation and the scattering geometry of the momentum resolved EELS experiment on a monolayer of graphene are shown schematically in fig. 1(d). In the experimental set-up fast electrons, with kinetic energy of up to 20 kV in this case, are transmitted through a free-standing graphene monolayer. The scattered electrons are analyzed with respect to the energy loss, $\hbar\omega$, they have undergone as a function of the scattering angle, θ, which is a measure of the momentum transfer $\hbar\boldsymbol{q}$. The momentum transfer $\hbar\boldsymbol{q}$, where the scattering vector $\boldsymbol{q}$, is given by $\boldsymbol{k}_0 - \boldsymbol{k}'$ in which case $\boldsymbol{k}_0$ and $\boldsymbol{k}'$ are the wave vectors of incident and inelastically scattered electrons (electrons that have undergone energy losses), respectively [33–35]. The vector $\boldsymbol{q}$ can be decomposed into $\boldsymbol{q}\,\|$, which is the component parallel to the electron beam direction (giving momentum transfer perpendicular to the graphene layer), and $\boldsymbol{q}\,\perp$ which is the component perpendicular to the electron beam (giving momentum transfer in the graphene layer plane). For $|\boldsymbol{q}| \ll |\boldsymbol{k}_0|$, then $\boldsymbol{q}\,\perp \approx \boldsymbol{k}_0 \sin\theta$ and $\boldsymbol{q}\,\| = \boldsymbol{k}_0(\Delta E/2E_0)$ with ΔE being the energy loss E_0, the energy of the incident electrons. For the energies losses of interest in this work ($0 \leqslant \Delta E \leqslant 10\,\text{eV}$), the quantity $\Delta E/2E_0$ is very small and hence the momentum transfer is in the graphene layer plane ($\boldsymbol{q}\,\perp$) [34].

Results and discussion. – Figure 2(a) presents a momentum resolved EELS spectrum showing energy loss (horizontal axis) as a function of momentum $|\boldsymbol{q}|$ (vertical axis). Individual EELS spectra at specific $|\boldsymbol{q}|$ values were obtained by acquiring integrated intensity profiles from the EELS spectrum shown in fig. 2(a). The obtained spectra were processed in order to subtract the background due to elastic scattering. Here the zero-loss peak was extracted from individual spectra by fitting the background with a power law as shown in fig. 2(b) [36]. In fig. 2(b) the elastic background is shown by the dashed blue curve, the raw spectra by the solid red curve and the background subtracted spectra by the dotted black curve. The area in the reciprocal space investigated in this EELS experiment ($\pm|\boldsymbol{q}| = \pm 2.95\,\text{Å}^{-1}$) is considerably larger than the typical dimension of the graphene's Brillouin zone in the Γ-M direction ($\sim 1.5\,\text{Å}^{-1}$). However, with increasing momentum transfer, the intensity of the energy losses shows a quadratic decay, *i.e.* the spectra at $0.2\,\text{Å}^{-1}$ is at least four times lower than at $0.1\,\text{Å}^{-1}$. To obtain spectra with a good signal to noise ratio we therefore concentrated on spectral data in the range $0 \leqslant |\boldsymbol{q}| \leqslant 0.5\,\text{Å}^{-1}$. Figure 2(c) shows the background subtracted EELS spectra for momentum transfers $0 \leqslant |\boldsymbol{q}| \leqslant 0.5\,\text{Å}^{-1}$. We observe three peak features in the EELS spectra of monolayer graphene.

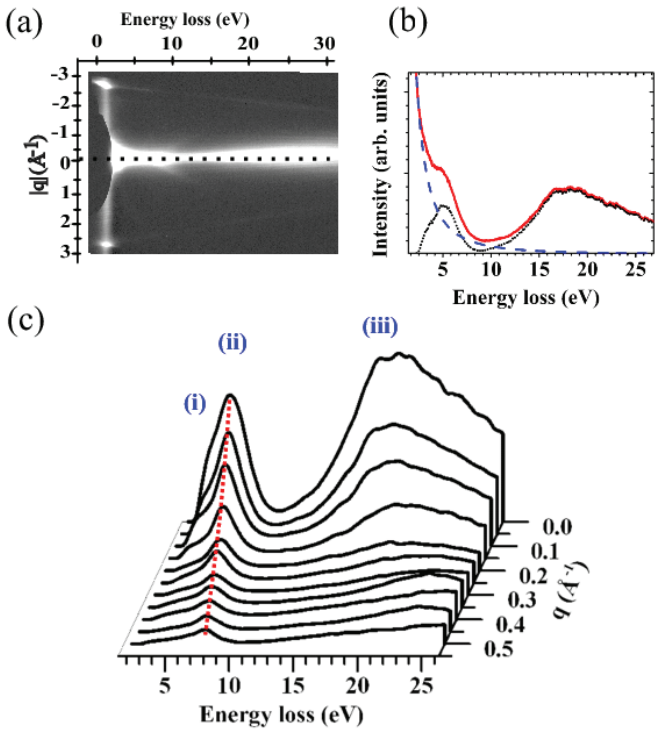

Fig. 2: (a) Momentum-resolved EELS spectrum for monolayer graphene showing energy loss (horizontal axis) *vs.* momentum $|\boldsymbol{q}|$ (vertical axis). (b) Obtaining the background-subtracted spectra (dotted black curve) by substracting the elastic background (dashed blue curve) from the raw spectra (solid red curve). (c) Background-subtracted EELS spectrum for $0 \leqslant |\boldsymbol{q}| \leqslant 0.5\,\text{Å}^{-1}$. The dotted line is a guide for the eye. The features labeled i), ii) and iii) are attributed to $\pi \to \pi^*$ interband transitions, π and $\pi + \sigma$ plasmon excitations, respectively.

These have been labelled as peak features i), ii) and iii). The first structure i), is a broad shoulder which is observed on the lower-energy range (<4 eV) of the EELS spectrum. For momentum transfers in the graphene layer plane, only interband transitions between states with same parity ($\pi \to \pi^*$ and σ^*) are allowed. On the other hand for momentum transfers perpendicular to the layers only interband transitions between states with different parity ($\pi \to \sigma^*$ and $\sigma \to \pi^*$, respectively) are allowed [16,37]. Therefore, the only allowed transitions below 10 eV are the $\pi \to \pi^*$ interband transitions. The $\sigma \to \sigma^*$ transitions are, on the other hand, usually expected to occur above 10 eV. Regarding a detailed discussion of the origin of the individual features the low-energy structure i) is related to $\pi \to \pi^*$ interband transitions across the "Dirac" cone at the K and K' points, respectively. With increasing momentum transfer at the "Dirac" point a gap opens and additional interband transitions across this gap are allowed and increase in intensity due to the increasing number of electronic states at the circumference of the "Dirac" cone. We point out that, although we did not measure in the Γ-K

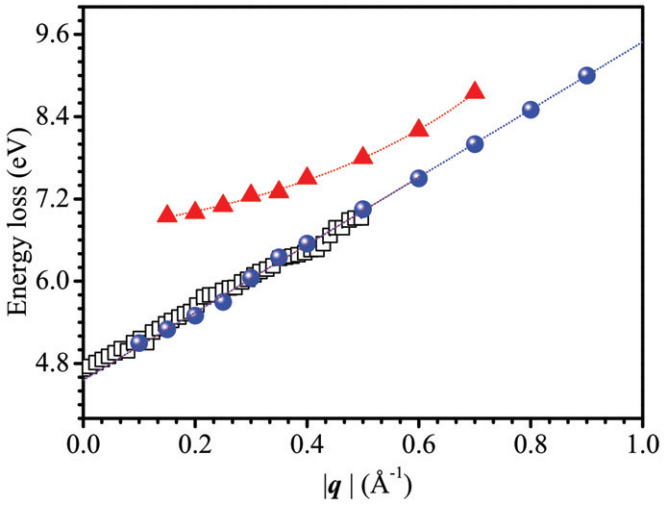

Fig. 3: Experimental dispersion of the π plasmon peak in a free-standing graphene monolayer (open squares), compared with experimental dispersion of π plasmon peak in vertically aligned single-wall carbon nanotubes (VA-SWCNT) (filled blue spheres) and graphite (filled red triangles). The dotted curves show the fits of the dispersion curves.

direction, we still have to include the transitions in this direction to describe the correct loss function. We have to take the excitations near the K-point into account because one has to integrate over all possible allowed interband transitions parallel to the measured vector $\boldsymbol{q}$. A direct assignment of individual transitions on a predefined symmetry direction therefore has to be done with some precaution. The second ii) and third peaks iii) are commonly observed in all graphitic carbons and are attributed to the π and $\pi+\sigma$ plasmons, respectively [38–43]. Similar to all other sp^2 derived carbon systems the peak width of both π and $\pi+\sigma$ plasmon peaks strongly increases with increasing momentum transfer. The width of the $\pi+\sigma$ peak is observed to increase more rapidly than the π plasmon peak. In addition, the position of the plasmon peaks disperses to higher energies as $|\boldsymbol{q}|$ increases. The π plasmon dispersion at low momentum transfer is of particular interest since it is related to all optical interband excitations. The dispersion of the π plasmon peak in graphene (open squares) is shown in fig. 3. The π plasmon dispersion in graphite (filled red triangles) [38], and vertically aligned single-wall carbon nanotubes, VA-SWCNT, (filled blue spheres) [3] are also shown for comparison. The π plasmon excitations in both VA-SWCNT and monolayer graphene can be described as showing linear momentum dependence. This is in contrast to the dispersion observed for graphite which shows the typical parabolic behaviour [38]. In graphite, this peak is due to respective interband transitions at the M-point and its dispersion is parabolic and can be described within a model of "quasi-free" electrons above interband transitions [41,42]. A linear fit of the dispersion curves for the monolayer graphene and SWCNT gives a plasmon energy of 4.61 eV for SWCNT and 4.7 eV for monolayer graphene at the optical limit, $|\boldsymbol{q}| \approx 0$ Å^{-1}. In comparison, the energy of the π plasmon peak in monolayer graphene has been determined to be 4.62 eV through optical measurements [15]. The slopes for the graphene and SWCNT curves are determined to be 4.53 eVÅ and 4.86 eVÅ, respectively. This is close to the calculated dispersion of interband transitions across the "Dirac" cone at the K-point. However, as pointed out in ref. [3] the energy range for the π plasmon (4–8 eV) is higher than the linear region of the Dirac cone (0.5 eV–4 eV). A possible explanation for the linear behaviour of the π plasmon for the energy range beyond the Dirac cone in free-standing graphene monolayers (and those on weakly interacting substrates) was provided by Kramberger *et al.* based on theoretical calculation of the energy-loss function for free-standing monolayer graphene and SWCNT [3]. The energy-loss function (ELF) is the quantity obtained from an EELS experiment and is proportional to minus the imaginary part of the inverse macroscopic dielectric function ELF $(q,\omega) = -\mathrm{Im}\,\varepsilon_M^{-1}(q,\omega)$. Kramberger *et al.* calculated the energy-loss function within the random phase approximation (RPA) both with and without the inclusion of the local-field effects. Within RPA one obtains the energy-loss function from the dielectric response of non-interacting electrons to external and induced fields. However, the dielectric response calculated in RPA without the inclusion of the local-field effects corresponds to response of a homogeneous material. In low-dimensional systems such as monolayer graphene and carbon nanotubes, and in periodic crystalline systems the valence electron density is inhomogenous. This inhomonegeneity in the electron density gives rise to local-field effects in the dielectric response [37,44]. Therefore, RPA without the inclusion of the local-field effects does not account for the variations in the dielectric response as a result of the inhomogeneity in the electron density on the atomic scale. Kramberger *et al.* showed that without the inclusion of local-field effects, the $\pi \to \pi^*$ transitions within the Dirac cone (from 0.5 eV up to 4 eV) in free-standing graphene monolayers have a linear dispersion. This is attributed to the band structure effects since the Dirac cone is linear in this energy range. The transitions at the edge of the Brillouin zone, however, showed a quadratic dispersion at low $|\boldsymbol{q}|$ values. With the inclusion of the local-field effects the low-energy transitions are completely suppressed and quadratic dispersion of the transitions beyond the Dirac cone is transformed to a linear dispersion. Inclusion of the local-field effects in the calculation leads to the mixture of transitions in the BZ of monolayer graphene. The linear dispersion of the $\pi \to \pi^*$ transitions is then explained as resulting from the supersposition of electron transitions originating at both the K and M points of the BZ. Therefore, the linear dispersion of the π plasmon in free-standing monolayer graphene reflects the momentum dependence of the $\pi \to \pi^*$ interband

transitions, the character of π and π^* bands along the Γ-M direction in graphene and the low-energy interband transitions across the "Dirac cone". Interestingly, the dispersion of the π plasmon in epitaxial graphene on SiC (0001) substrate has been also shown to be linear, which agrees with our results for free-standing graphene [18]. However, based on theoretical calculations Yan *et al.* [8] have shown that the π plasmon is significantly damped on a SiC (0001) substrate although its energy remains unaltered. A similar linear behaviour is also observed for low-energy plasmons in epitaxial graphene for the cases where the interaction between the substrate and graphene is weak. This has been shown for epitaxial graphene on Ir (111) [11], and Pt (111) [13], and Au/Ni (111) [14]. In this case the graphene electronic properties are not affected by the substrate and the graphene sheet can be considered to be quasi-free standing. A different behaviour is however observed for epitaxial graphene on SiC (0001) [9,10,12] and Ni (111) [14] substrates. In this case, at low momentum values the dispersion of low-energy plasmons is similar to a classical two-dimensional electron gas (2DEG) showing a $\omega_p \propto q^{1/2}$ dependency, where ω_p is the plasmon frequency. However, at larger momentum values the dispersion deviates from this classical 2DEG behaviour displaying a linear behaviour. The dispersion behaviour of the π plasmons in free-standing graphene presented here shows that the π plasmons in graphene and SWCNT are not pure plasmon excitations in the classical sense but are a result of all $\pi \to \pi^*$ interband transitions. We observe a linear behavior of the π plasmons in free-standing graphene monolayers and that at low relative momentum transfer the low-energy interband excitations play a crucial role. Therefore, our TEM-EELS results on free-standing graphene are in agreement with previous theoretical calculations for free-standing graphene [3] and with previous high-resolution reflection electron energy-loss spectroscopy (HREELS) results on epitaxial graphene on SiC [18].

Conclusion. – In conclusion, we have investigated the dispersion properties of π plasmons in free-standing monolayer graphene using momentum-resolved electron energy-loss spectroscopy. We have focused on the momentum range $0 \leqslant |\boldsymbol{q}| \leqslant 0.5\,\text{Å}^{-1}$ and parallel to the Γ-M direction of the graphene Brillouin zone. We have shown that the dispersion of the π plasmons in free-standing monolayer graphene is characterized by a linear dispersion. This linear dispersion of the π plasmons is shown to be similar to the one observed for single-wall carbon nanotubes. We conclude that the character of the π plasmons in monolayer graphene is attributed to the $\pi \to \pi^*$ interband transitions within the measured energy range.

* * *

We gratefully acknowledge financial support by the German Research Foundation (DFG) and the Ministry of Science, Research and the Arts (MWK) of the state Baden-Württemberg within the Sub-Angstrom Low-Voltage Electron Microscopy project (SALVE). The work in Vienna was supported by the FWF project FWF-I377–N16. CK acknowledges the APART fellowship 11456 of the Austrian Academy of Science.

REFERENCES

[1] Novoselov K. S., Geim A. K., Morozov S. V., Jiang D., Katsnelson M. I., Grigorieva I. V., Dubonos S. V. and Firsov A. A., *Nature (London)*, **438** (2005) 197.
[2] Castro-Neto A. H., Peres N. M. R., Novoselov K. S. and Geim A. K., *Rev. Mod. Phys.*, **81** (2009) 109.
[3] Kramberger C., Hambach R., Giorgetti C., Rümmeli M., Knupfer M., Fink J., Büchner B., Reining L., Einarsson E., Maruyama S. *et al.*, *Phys. Rev. Lett.*, **100** (2008) 196803.
[4] Chuvilin A., Kaiser U., Bichoutskaia E., Besley N. A. and Khlobystov A. N., *Nat. Chem.*, **2** (2010) 450.
[5] Dresselhaus M. S., Jorio A. and Saito R., *Annu. Rev. Condens. Matter Phys.*, **1** (2010) 89.
[6] Hwang E. H. and Das Sarma S., *Phys. Rev. B*, **75** (2007) 205418.
[7] Hwang E., Sensarma R. and Das Sarma S., *Phys. Rev. B*, **82** (2010) 195406.
[8] Yan J., Thygesen K. and Jacobsen K., *Phys. Rev. Lett.*, **106** (2011) 146803.
[9] Liu Y., Willis R., Emtsev K. and Seyller T., *Phys. Rev. B*, **78** (2008) 201403.
[10] Tegenkamp C., Pfnür H., Langer T., Baringhaus J. and Schumacher H. W., *J. Phys.: Condens. Matter*, **23** (2011) 012001.
[11] Langer T., Förster D. F., Busse C., Michely T., Pfnür H. and Tegenkamp C., *New J. Phys.*, **12** (2011) 053006.
[12] Koch R., Seyller T. and Schaefer J., *Phys. Rev. B*, **82** (2010) 201413(R).
[13] Politano A., Marino A., Formoso V., Farías D., Miranda R. and Chiarello G., *Phys. Rev. B*, **84** (2011) 033401.
[14] Generalov A. V. and Dedkov Yu. S., *Carbon*, **50** (2012) 183.
[15] Mak K. F., Shan J. and Heinz T., *Phys. Rev. Lett.*, **106** (2011) 046401.
[16] Eberlein T., Bangert U., Nair R., Jones R., Gass M., Bleloch A., Novoselov K., Geim A. and Briddon P., *Phys. Rev. B*, **77** (2008) 233406.
[17] Yuan S., Roldán R. and Katsnelson M., *Phys. Rev. B*, **84** (2011) 035439.
[18] Lu J., Loh K., Huang H., Chen W. and Wee A., *Phys. Rev. B*, **80** (2009) 113410.
[19] Hill A., Mikhailov S. A. and Ziegler K., *EPL*, **87** (2009) 27005.
[20] Stern F., *Phys. Rev. Lett.*, **18** (1967) 546.
[21] Pines D., *Rev. Mod. Phys.*, **28** (1956) 184.
[22] Ozbay E., *Science*, **311** (2006) 189.
[23] Chen C. H., *J. Phys. C: Solid State Phys.*, **9** (1976) L321.

[24] Pettit R., Silcox J. and Vincent R., *Phys. Rev. B*, **11** (1975) 3116.
[25] Midgley P., *Ultramicroscopy*, **76** (1999) 91.
[26] Novoselov K. S., Geim A. K., Morozov S. V., Jiang D., Zhang Y., Dubonos S. V., Grigorieva I. V. and Firsov A. A., *Science (N.Y.)*, **306** (2004) 666.
[27] Meyer J. C., Girit C. O., Crommie M. F. and Zettl A., *Appl. Phys. Lett.*, **92** (2008) 123110.
[28] Kaiser U., Biskupek J., Meyer J. C., Leschner J., Lechner L., Rose H., Stöger-Pollach M., Khlobystov A. N., Hartel P., Müller H. *et al.*, *Ultramicroscopy*, **111** (2011) 1246.
[29] Meyer J. C., Geim A., Katsnelson M., Novoselov K., Obergfell D., Ro S., Girit C. and Zettl A., *Solid State Commun.*, **143** (2007) 101.
[30] Leapman R., Fejes P. and Silcox J., *Phys. Rev. B*, **28** (1983) 2361.
[31] Tarrio C. and Schnatterly S., *Phys. Rev. B*, **40** (1989) 7852.
[32] Ritsko J., *Phys. Rev. B*, **25** (1982) 6452.
[33] Egerton R. G., *Electron Energy-loss Spectroscopy in the Electron Microscope* (Plenum Press, New York) 1986, p. 131.
[34] Fink J., *Adv. Electron. Electron Phys.*, **75** (1989) 121.
[35] Schattschneider P., *Ultramicroscopy*, **28** (1989) 1.
[36] Erni R. and Browning N. D., *Ultramicroscopy*, **104** (2005) 176.
[37] Trevisanutto P., Giorgetti C., Reining L., Ladisa M. and Olevano V., *Phys. Rev. Lett.*, **101** (2008) 226405.
[38] Zeppenfeld K., *Z. Phys. A*, **211** (1971) 391.
[39] Taft E. and Philipp H., *Phys. Rev.*, **138** (1965) A197.
[40] Tosatti E. and Bassani F., *Nuovo Cimento B*, **65** (1970) 161.
[41] Lin M. F., Huang C. S. and Chuu D. S., *Phys. Rev. B*, **55** (1997) 13961.
[42] Marinopoulos A., Reining L., Rubio A. and Olevano V., *Phys. Rev. B*, **69** (2004) 245419.
[43] Venghaus H., *Phys. Status Solidi (b)*, **66** (1974) 145.
[44] Sturm K., *Adv. Phys.*, **31** (1982) 1.